Desalination and Water Treatment
www.deswater.com

doi:10.5004/dwt.2021.27285

227 (2021) 412–424
July

Evaluation of olive pomace for the separation of anionic dyes from aqueous solutions: kinetic, thermodynamic, and isotherm studies

Khalid Ali[a], Hani Zeidan[a,b], Mustafa Esen Martı[a,b,*,†]

[a]*Department of Chemical Engineering, Selçuk University, Konya, Turkey, emails: marti@selcuk.edu.tr/memarti@ktun.edu.tr/ mustafaesenmarti@gmail.com (M.E. Marti), khalid_unit@yahoo.com (K. Ali), hani-z82@hotmail.com (H. Zeidan)*
[b]*Department of Chemical Engineering, Konya Technical University, Konya, Turkey*

Received 10 August 2020; Accepted 3 April 2021

ABSTRACT

Today, water pollution is one of the major problems threatening human health. Synthetic dyes from industrial effluents are among the many toxic compounds that cause water pollution. The aim of this study is the evaluation of olive pomace (OP) to be used as a biosorbent during the separation of two anionic dyes, Congo Red (CR) and Methyl Orange (MO), from aqueous solutions by adsorption technique. The biosorbent was characterized using Fourier transform infrared, Brunauer–Emmett–Teller, Barrett–Joyner–Halenda, and scanning electron microscopy with energy-dispersive X-ray spectroscopy. It was shown to be largely unaffected by pH, indicating that OP can be utilized over a wide pH range. Experiments were conducted without pH adjustment of aqueous solutions. Kinetics showed that adsorption followed the pseudo-second-order kinetic model and reached equilibrium in 210 min. Efficiency reduced with the increase in temperature and thermodynamic parameters indicated that physical or physico-chemical interactions may have occurred between the dyes and OP. The process was exothermic and non-spontaneous. The efficiency was negatively influenced by initial dye concentration while positively affected by the OP dose. The trend was reversed for adsorption capacity, resulting in maximum values of 145.0 and 257.4 mg/g for CR and MO, respectively. These were higher than those reported in the literature for the sorption of these dyes using various types of waste materials. The process was well-explained by Freundlich isotherm for both dyes. The OP was found to be effective for the separation of anionic dyes from aqueous solutions over wide pH and concentration ranges.

Keywords: Olive pomace; Adsorption; Congo Red; Methyl Orange; Anionic dyes; Separation

1. Introduction

Water pollution is one of the most serious environmental concerns given the role water plays in our lives. Beyond its need for drinking, cooking, and bathing, it is used in all major industries and agriculture [1]. Over the years, the quality of freshwater has deteriorated due to the emergence and use of various types of pollutants. These waste materials are severely hazardous and cause critical health problems for human beings, animals, and plants.

Today, nearly one million tons of synthetic dyes are manufactured each year and more than 100,000 types of dyes are in commercial use. Following their use, nearly 10%–15% of these accumulate in wastewaters from which they are released to the environment and natural resources [2]. Fortunately, there are several processes that can be effectively used to remove these toxic chemicals from aquatic environments. Adsorption has been proposed to be one of the most effective separation methods for the removal of hazardous materials such as synthetic dyes, heavy metals, and pesticides because of its high efficiency, low-cost, and simplicity

* Corresponding author.

[†]Present address: Konya Technical University, Konya, Turkey, Tel. +90-332-223-1837; Fax: +90-332-241-0635

[3]. The method could be more advantageous if the total cost could be reduced by employing low-cost adsorbents.

There are many publications in the literature on the evaluation of waste materials, by-products, or low-cost adsorbents for the separation of synthetic dyes from wastewaters or other aqueous solutions. Most of these sorbents are agricultural by-products and industrial wastes [4–7]. Since the need for efficient and low-cost adsorbents to be used in the adsorptive separation is growing, research to find new alternatives is continuing [8–10].

Olive pomace (OP) is one of these alternatives. Olive oil production results in a by-product consisting of water, oil, and pomace solids (50%, 30%, and 20% by wt., respectively). Since olives and olive oil are key agricultural products in Mediterranean region, OP is abundant in the countries of this geographical area. Unfortunately, as it has limited use in industry, most of the solid residue from olive oil processing is blended with agricultural soil [11]. However, it could be used instead for removing toxic wastes from the environment.

It has been previously shown that OP can be employed for the removal of heavy metals and cationic dyes. Compared with granular activated carbon, its low-cost is an attractive advantage [11–14]. Pagnanelli et al. [11] removed heavy metals (Pb, Cu, and Cd) from contaminated aqueous solutions using OP. The researchers observed that hydrogen ions competed with the heavy metals for the adsorption onto OP [11]. In another study, the authors modeled the co-adsorption of Cu and Cd on OP and noticed a competition between these metals for this adsorbent [15]. The effects of temperature, adsorbate concentration, adsorbent dosages, pH, and agitation rate on the nickel (Ni(II)) separation by OP were studied by Nuhoğlu and Malkoç [13]. They achieved the maximum adsorption capacity at pH = 4, and the process was well-explained by Temkin and Langmuir models [13].

Recently, OP was tested for the separation of synthetic dyes from aqueous media. Akar et al. [16] used OP to remove Reactive Red 198 from aqueous solutions and showed that equilibrium was reached after 40 min. The maximum adsorption capacity (q_{max} = 44.23 mg/g) was obtained at pH = 2. Bozkan [17] studied the separation of two cationic dyes from aqueous solutions and attained the maximum separation capacities of 163.0 and 354.1 mg/g for methylene blue and crystal violet, respectively. Dağdelen et al. [18] achieved a maximum separation capacity of 23.63 mg/g for the adsorption of Remazol Brilliant Blue R onto OP. The authors mentioned that pH = 3 and 50°C were optimum conditions for the process [18]. Koçer and Acemioğlu [19] reported that efficiency increased with the concentration, temperature, and pH, but decreased with the ionic strength for the removal of Basic Green-4. The data were explained using the Langmuir isotherm (q_{max} = 41.66 mg/g) and pseudo-second-order kinetic model. Oden et al. [20] obtained an adsorption efficiency of 80% and a capacity of 17.5 mg/g for the removal of Everzol Yellow 3RS at pH = 7.5, 298 K, and 150 min contact time [20]. Finally, Beaj et al. [21] used OP (20–120 g/L) to remove Methyl Orange (MO) from dilute (2.5–20 mg/L) aqueous solutions. The highest efficiency was obtained at pH = 2 and 80 min equilibration time. Adsorption kinetics were consistent with the pseudo-second-order kinetic model, and equilibrium data were in good agreement with the Freundlich isotherm model [21].

In this study, an agricultural by-product, OP, was evaluated for use in the separation of two anionic dyes, Congo Red (CR) and Methyl Orange (MO) from aqueous solutions. These dyes are employed in various applications and are similar to several types of dyes that have been used in industry. The separation efficiencies obtained for these dyes were compared with each other and with the corresponding data previously reported in the literature. Another significant goal of this study was to probe the effects of separation variables such as initial pH, contact time, temperature, dye concentration, and OP dose on the efficiency and adsorption capacity. In addition, isotherm- and kinetic models were applied to explain the adsorption mechanism. Finally, the constants of the models and thermodynamic parameters were determined using the experimental data.

2. Materials and methods

2.1. Materials

The OP (Fig. 1) was obtained from an olive oil production factory in southern Turkey. It was dried and sieved (particle size < 53 mesh) and used without further treatment. Methyl Orange (MO, $C_{14}H_{14}N_3NaO_3S$) and Congo Red (CR, $C_{23}H_{22}N_6O_6S_2Na_2$,) were utilized as the model anionic dyes to be removed from aqueous solutions. The molecular structures of MO and CR are shown in Fig. 2. The chemicals are listed in Table 1.

Fig. 1. Olive pomace was used as the adsorbent in this study.

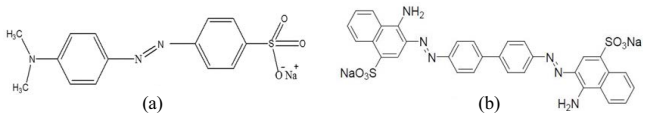

Fig. 2. Structures of the anionic dyes used in this study: (a) Methyl Orange and (b) Congo Red.

Table 1
Chemicals utilized in this study

Chemical	IUPAC name	Source	CAS #	Assay (%)
Congo Red	Disodium 4-amino-3-[4-[4-(1-amino-4-sulfonato-naphthalen-2-yl) diazenylphenyl] phenyl] diazenyl-naphthalene-1-sulfonate	Merck, USA	573-58-0	≥97
Methyl Orange	Sodium 4-{[4-(dimethylamino) phenyl]diazenyl} benzene-1-sulfonate	Merck, USA	547-58-0	≥97
Hydrochloric acid	Hydrochloric acid	Merck, USA	7647-01-0	37
Sodium hydroxide	Sodium hydroxide	Merck, USA	1310-73-2	≥99

2.2. Characterization and analysis

Fourier transformed infrared (FTIR) spectra of raw OP and dye-loaded OP were obtained using a Bruker Vertex 70 FTIR spectrometer (Bruker Co., Kassel, Germany). Samples were prepared as KBr pellets; spectra were collected over the range of 4,000–400 cm^{-1}. Adsorption–desorption isotherms of N_2 at 77 K were measured using a TriStar II-3020 nitrogen surface area/porosity analyzer (Micromeritics, USA). The surface areas and the pore size distributions were calculated by Brunauer–Emmett–Teller (BET) (Eq. (1)) and Barrett–Joyner–Halenda (BJH) methods, respectively [22,23].

$$\frac{\frac{P}{P_o}}{V\left(1-\frac{P}{P_o}\right)}=\frac{1}{V_m\cdot C}+\frac{C-1}{V_m\cdot C}\cdot\frac{P}{P_o} \tag{1}$$

where P and P_o are the equilibrium and the saturation pressure, respectively, of adsorbate at the temperature of adsorption, V is the adsorbed gas quantity (cm^3/g), V_m is the monolayer adsorbed gas quantity, and C is the BET constant.

The surface features and the ratio of the elements of OP were investigated by scanning electron microscopy (SEM, Zeiss EVO/LS10, Carl Zeiss AG Co., Germany) and energy-dispersive X-ray spectroscopy (EDX; Bruker 123 eV Quantax Microanalysis System, Bruker Co., Germany).

The concentrations of the synthetic dyes in the aqueous solutions were measured with a Shimadzu UVmini-1240 UV-Vis spectrophotometer (Shimadzu Co., Japan) using the Beer–Lambert relation (Eq. (2)):

$$\text{Absorbance}=\varepsilon\cdot C_s\cdot l \tag{2}$$

where ε is the molar extinction coefficient, C_s refers to the sample concentration and l is the path length (1 cm). The maximum (λ_{max}) absorbances were obtained at 464 and 497 nm for MO and CR, respectively.

2.3. Kinetic studies

In the kinetic experiments, 0.10 g of OP was added to the 50 mL Erlenmeyer flasks containing 10 mL of dye solutions having a concentration of 250 mg/L. The mixture was incubated in a constant temperature shaker bath (BS-21, Jeiotech Co., Korea). All experiments were started at the same time and the samples were removed from the bath at varying intervals over a period of 5 h. The samples were centrifuged at 4,000 g for 5 min (CompactStar CS4) and the supernatants containing the aqueous phases were recovered. Dye concentrations were determined using the spectrophotometer.

2.4. Thermodynamic studies

The effect of the temperature on the adsorption process was determined and thermodynamic parameters were calculated using the relevant data. The OP dose was 10 g/L and the system temperature was varied between 298 and 318 K. As with the kinetic studies, the samples were centrifuged and dye concentrations were determined as described above.

2.5. Equilibrium studies

Aqueous MO and CR solutions (100–5,000 mg/L) were prepared using ultra-high pure water, obtained from a Millipore Direct-Q 3V UHP Water System. Ten milliliters of each dye solution were contacted with the pre-determined dosages of OP (5–25 g/L) in 50 mL Erlenmeyer flasks and shaken at 150 rpm for 240 min. Then, the mixtures were centrifuged at 5,000 rpm for 5 min to separate the phases. The aqueous phases were carefully recovered from the flasks and dye concentrations were determined. The amount of dye adsorbed by OP was calculated by mass balance. Both adsorption capacity and efficiency were determined by utilizing Eqs. (3) and (4):

$$q_e=\left(\frac{C_0-C_e}{m}\right)\cdot V \tag{3}$$

$$\text{AE}(\%)=\left(\frac{C_0-C_e}{C_0}\right)\cdot 100 \tag{4}$$

where C_0 and C_e (mg/L) represent the initial and equilibrium concentrations of the dyes, respectively. The q_e (mg/g), m (g), V (L), and AE (%) are the adsorption capacity, mass of OP, volume of the aqueous solution, and adsorption efficiency, respectively.

The pH at which OP has a neutral surface (pH_{ZPC}) was determined by using the solid addition and zeta-potential methods [24–27]. In the former method, 45 mL of 10 mmol/L $NaNO_3$ solutions were added to a series of 100 mL Erlenmeyer flasks. The pH (pH_i) of the solutions was adjusted in the range 2–12 with 0.10 mol/L HCl or 0.10 mol/L NaOH. The total volumes of the solutions were adjusted to 50 mL with 10 mmol/L $NaNO_3$. 0.1 g of OP was added and the flasks were sealed and the suspensions were shaken in a constant temperature water bath at 298 K for 48 h. Then, the suspensions were centrifuged and the supernatants recovered. The pH values of the final supernatants (pH_f) were measured. The differences between the initial and final pH values ($\Delta pH = pH_f - pH_i$) were plotted vs. the initial pH. The *x*-intercept of the resulting curve was the pH_{ZPC}.

The samples for zeta potential analysis were prepared by mixing 0.1 g of OP with 50 mL deionized water adjusted to different pH values. The mixtures were sonicated for 12 h after which the zeta potential values were measured in the range of −12.5 to 251.5 mV. In order to determine the influence of aqueous pH on separation efficiency, experiments were conducted at initial pH values between pH = 2.5 and 10.5. The initial anionic dye concentration was adjusted to be 250 mg/L in these experiments. The initial pH values of these aqueous MO and CR solutions were found to be 5.8 and 6.6, respectively. Aqueous solutions of sodium hydroxide and hydrochloric acid were utilized for pH adjustment.

The adsorption mechanism was interpreted using the equilibrium data and three isotherm models. The relevant equations and comments are presented in the following sections.

3. Results and discussion

3.1. Characterization

The chemistry of the adsorbent may help to explain the mechanism of the adsorption process [4,9,28]. In this study, FTIR was employed to investigate the functional groups on the OP surface, and how they changed during the adsorptive separation. The FTIR spectra of the OP and loaded-OP (Fig. 3) indicate the presence of several types of functional groups. The broad peak observed between 3,200 and 3,400 cm^{-1} could be assigned to the O–H stretching vibrations. The peaks at 2,920 and 2,850 cm^{-1} were associated with C–H stretching vibrations of CH, CH_2, and CH_3 groups of lignin [29]. The signals at ~1,610 and 1,540 cm^{-1} showed the presence of carboxyl and amino groups stretching, respectively. The peak at 1,035 cm^{-1} may be due to vibrations of C-6 of cellulose [30]. The major peaks of raw OP are also in the spectra of the dye-loaded-OP. However, intensities of the peaks at 2,920; 2,850; and 1,035 cm^{-1} significantly reduced after the process. Furthermore, shifts in the wavenumbers of the related peaks were noticed. These results exhibit that OP has distinctive features that can be useful during the sorption of the CR and MO molecules.

Nitrogen adsorption–desorption isotherms of OP (Fig. 4a) with hysteresis loop (type IV) showed that OP is a mesoporous adsorbent (2–50 nm). The specific surface area of the OP, which was measured by the BET method and Eq. (1), was found to be 404.25 m^2/g (Fig. 4b). The total pore volume

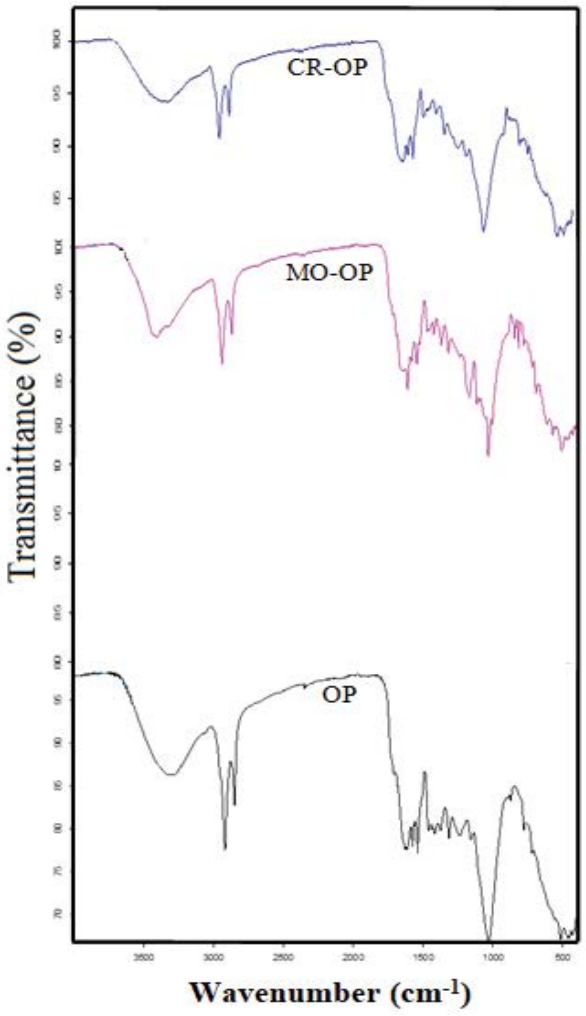

Fig. 3. FTIR spectra of OP and CR loaded- and MO loaded-OP.

of OP (obtained from the liquid volume of the N_2 adsorbate at a relative pressure of 0.95) was found to be 0.287 cm^3/g. Pore size distributions of OP powder (determined by the BJH method) are shown in Fig. 4c. The pore size distribution curve shows three peaks at 1.58, 1.95, and 2.38 nm indicating the generation of mesopores in the OP. The morphology of the OP used in the experiments was analyzed by SEM. The SEM images of the raw or unloaded- and dye-loaded-OP samples are shown in Fig. 5. The porous structure of the biomass can be clearly seen in the image of the unloaded OP. The biosorbent has surface cavities capable of adsorbing dye molecules. This capability is important because of the possible increase in the area and adhesion power of the surface [31]. The SEM images of the dye-loaded-OP exhibit a tendency to form agglomerates. It can be said that the features of the OP surface changed with the adsorption of the anionic dyes [32]. The differences in the surface morphologies of the raw OP and loaded-OP indicated the presence of the adsorbate molecules on the OP.

The chemical composition of OP (as determined by SEM-EDX, Fig. 6) is listed in Table 2. Oxygen and carbon account for the highest percentages and more than 90% of the OP

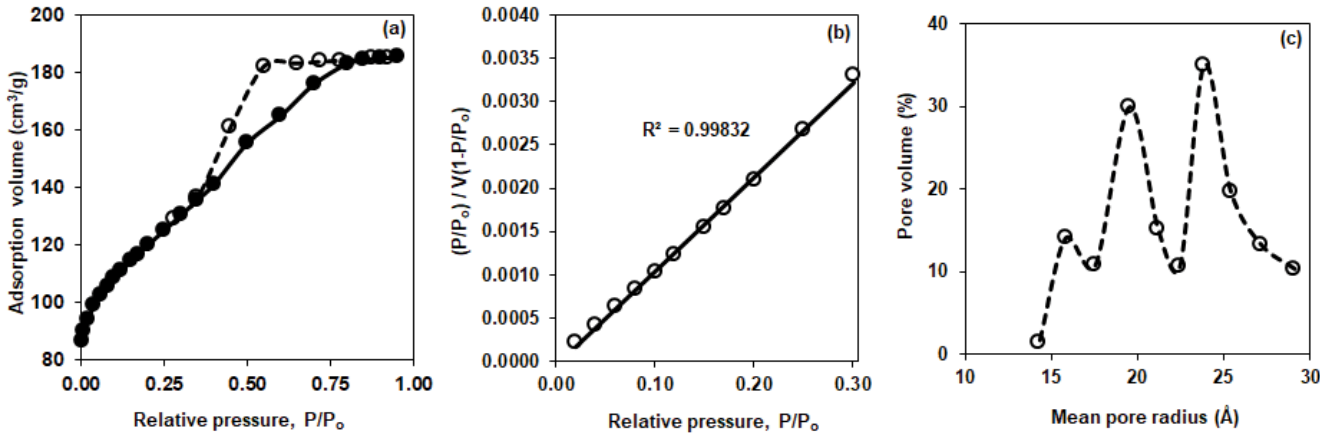

Fig. 4. (a) Nitrogen adsorption–desorption isotherms, (b) application of the BET equation, and (c) BJH pore size distribution curves for the adsorption of N_2 on OP at 77 K.

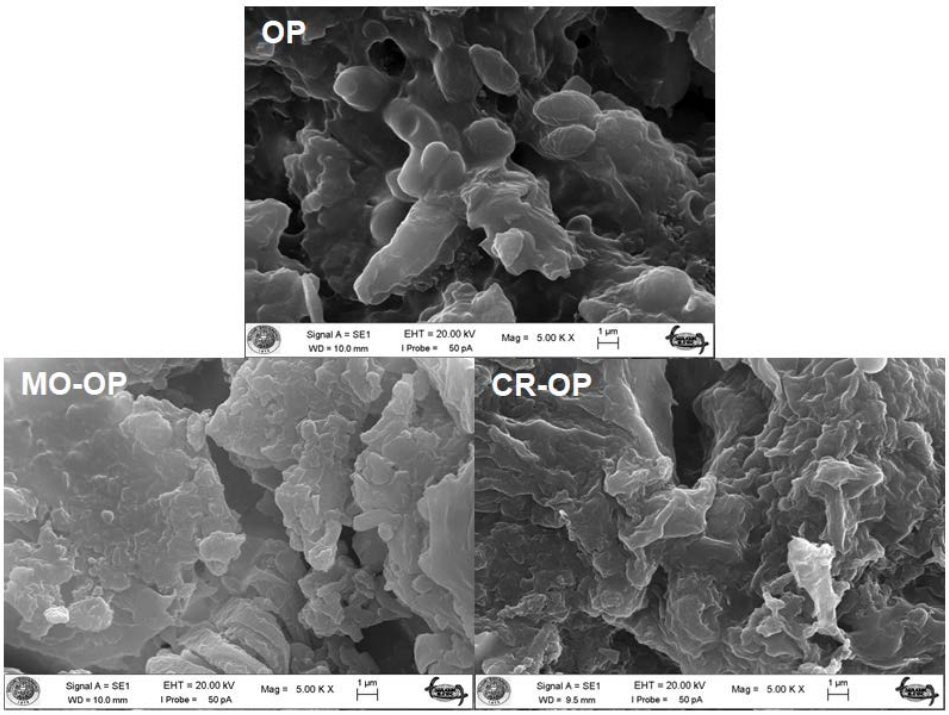

Fig. 5. SEM images of OP and CR loaded- and MO loaded-OP samples.

consists of these two elements. Calcium, potassium, magnesium, and aluminum account for about 5.5%.

3.2. Effect of pH

One of the most important parameters in the adsorption process is the pH of the media. The chemistry of the adsorbate and functional groups of the adsorbent can be influenced by the solution pH. Moreover, the color intensity in the aqueous phase may change depending on the structural stability of the dye molecule, which is also affected by pH [33]. In these experiments, the effect of initial pH on the separation of MO and CR using OP was tested from pH = 2.5 to 10.5 (Fig. 7a). The pH of the MO and CR solutions having the concentration of 250 mg/L were measured to be 5.8 and 6.6, respectively.

The effect of solution pH on the dye uptake can be explained based on the pH at point zero charge (pH_{ZPC}) of the adsorbent [25,27,34]. This was determined by pH drift and zeta potential measurements. At pH < pH_{ZPC}, the OP surface has a predominance of positive charges that adsorbs anionic dyes; and at pH > pH_{ZPC} the surface is negatively charged and adsorbs cationic dyes. The pH_{ZPC} shows that the net charge of OP is zero at about pH = 9.0 (Figs. 7b and c). Below pH = 9.0,

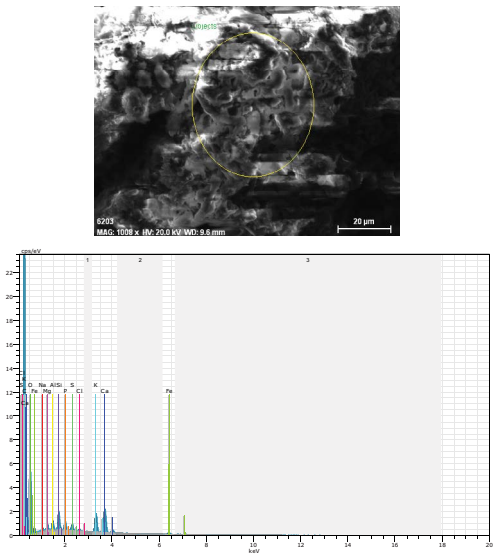

Fig. 6. SEM-EDX micrograph of OP.

Table 2
Elemental composition of OP (SEM-EDX results)

Element	(wt.%)
C	42.75
O	48.68
Ca	2.73
K	1.64
Mg	0.63
Al	0.55
P	0.55
S	0.38
Si	0.91
Cl	0.16
Fe	0.45
Na	0.57

positive charges predominate on the OP surface, enhancing the electrostatic interaction between the OP and the anionic dyes. Above pH = 9.0, the charge of the adsorbent surface was negative, causing electrostatic repulsion between OH^- and dye ions, preventing their adsorption by OP.

Table 3 shows that the influence of aqueous pH on the separation of CR and MO was not significant ($p > 0.05$ and $f < 5$). The maximum removal of MO (79.6%) was obtained at pH = 2.5 and the efficiency was 73.4% at the natural (unadjusted) pH (pH = 5.8) of the solution. Within the range studied, the efficiency decreased from 79.6% (pH = 2.5) to 67.6% (pH = 10.5), possibly due to the electrostatic interactions between MO and the partial negative charge on the adsorbent surface at pH > pH_{ZPC}~9.0 [35,36]. According to Fig. 7, the efficiencies for MO were higher than for CR. A possible explanation is that the lower molecular weight of MO (327.34 g/mol) facilitates its adsorption compared with CR (696.68 g/mol). The maximum adsorption efficiency for CR (50.8%) was at pH = 5.5 compared to 48.2% at the natural (unadjusted) pH (pH = 6.6) of the

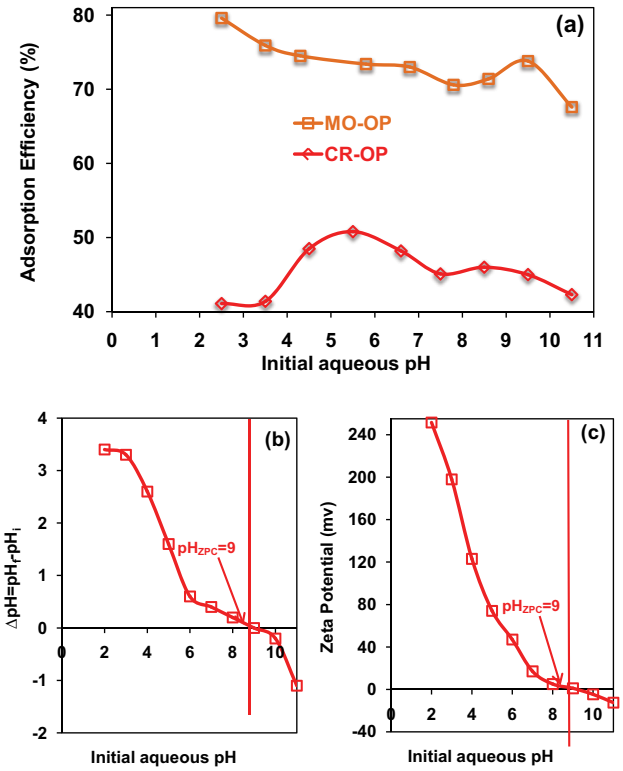

Fig. 7. (a) Influence of aqueous pH on the adsorption efficiency of MO and CR by OP, (b) determination of the zero-point charge (pH_{ZPC}), and (c) zeta potential of OP (initial dye concentration: 250 mg/L, OP dose: 10 g/L, and temperature: 298 K).

CR solution. Decreasing the pH to pH = 2.5 had a negative effect on separation efficiency. Similarly, raising the pH to pH = 10.5 > pH_{ZPC}~9.0 reduced the efficiency to 42.3%. Acids and bases used to modify the pH may compete with CR adsorption onto OP [36]. These observations are consistent with the results in the literature [19,21,37].

In summary, the initial pH did not considerably influence the efficiency of the adsorption process for either anionic dye. This means that the OP can be effectively used over a wide pH range. Hence, the following experiments were conducted with the MO and CR solutions without pH adjustment.

3.3. Effect of contact time

Another critical parameter for the design of a separation system is contact time [38]. This is the time required for adsorption to reach the equilibrium and must be determined in advance [39]. The results of the kinetic studies for the adsorption of MO or CR from aqueous phases using OP are presented in Fig. 8. In these experiments, the dye concentrations were about 250 mg/L while the OP dose was 10 g/L. As observed in the previous section, the separation efficiencies obtained with MO were obviously higher than the ones with CR.

For both dyes, adsorption equilibria were achieved by 210 min. The adsorption process occurred in two stages. The first stage was rapid, lasting about 20 min, resulting in efficiencies of 55.9% and 30% for MO and CR, respectively. The second stage was slower and took about 190 min.

The separation efficiencies were 73.4% and 48.2%, respectively, when the systems reached the equilibrium. Initially there was no dye on the OP surface and all sites were available for adsorption. However, in the second stage, most of the sites were filled with the solute molecules and the remaining available sites were inaccessible owing to the repulsive forces between the dye molecules [40].

3.4. Effect of initial dye concentration and OP dosage

The effects of the initial OP dosage and the dye (MO or CR) concentration on the adsorption capacity are shown in Fig. 9. Influence of initial MO and CR concentration was observed in the range of 100 and 5,000 mg/L while the OP dosage was between 5 and 25 g/L. The initial pH of the MO and CR solutions were not adjusted and the contact time was 240 min at 298 K.

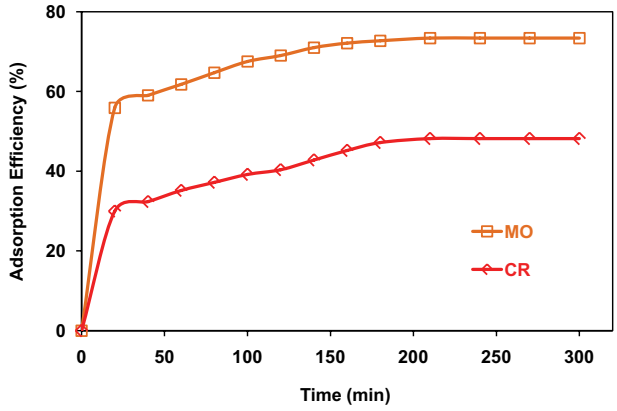

Fig. 8. Influence of contact time on the adsorption efficiency of MO and CR by using OP (initial dye concentration: 250 mg/L, OP dose: 10 g/L, and temperature: 298 K).

The results indicate that adsorption capacity (q_e) increased with MO and CR concentrations and decreased with OP dose. However, it was reversed for the separation efficiency ($p << 0.05$ and $f >> 5$, Table 3). As previously reported, the separation efficiency increased with the OP dose due to the increased surface area and the number of available binding sites [41]. However, it decreased with adsorbate concentration for both dyes due to the increasing ratio of dye molecules to the available adsorbent surface area [42]. The highest removal efficiencies were 86.8% and 88.2% for MO and CR, respectively, in the range of the concentrations and dosages tested. Maximum q_e values were 257.4 and 145.0 mg/g for MO and CR, respectively, and were obtained at 5 g/L OP dose and 5,000 mg/L dye concentration. The adsorption capacities with MO were notably higher than those for CR, possibly due to the relatively small size of the former dye. Alternatively, steric effects could decrease the sorption of CR by OP. These maximum adsorption capacities observed here were in the range of the values reported in the literature, in which OP was used as the adsorbent for the removal of synthetic dyes from aqueous solutions [16–21]. Furthermore, data in Table 4 show that these capacities were higher than the values previously reported in the studies using different types of waste materials for the adsorption of MO and CR [42–53].

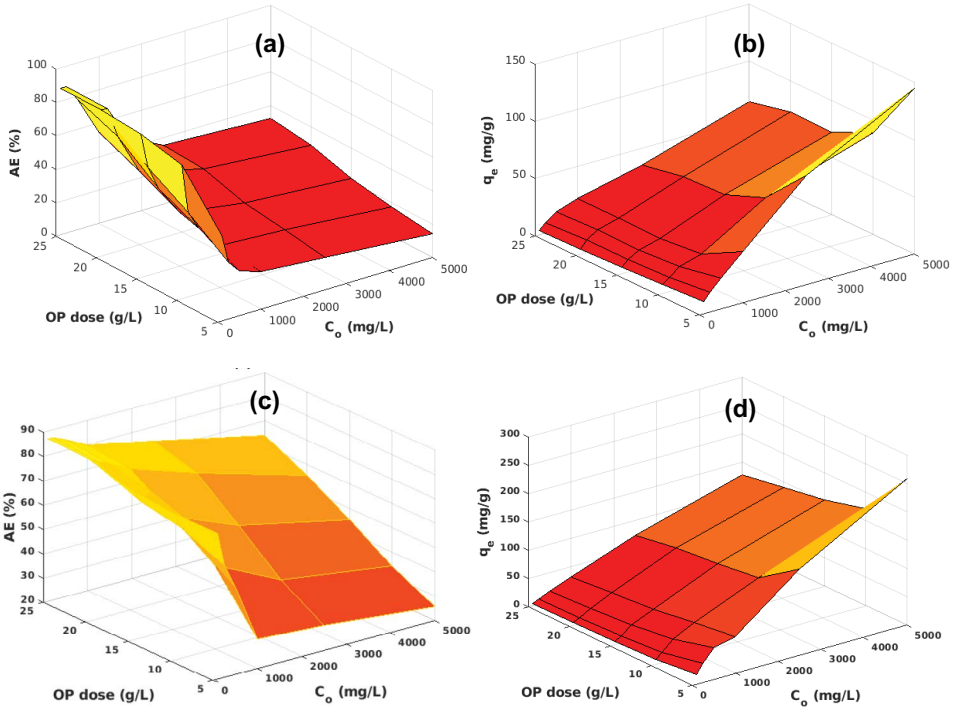

Fig. 9. 3D surface plots for the effects of adsorbent dose and dye concentration on the adsorption efficiency and capacity for the removal of MO and CR by OP: (a) AE(%)-CR, (b) q_e-CR, (c) AE(%)-MO, and (d) q_e-MO (initial dye concentration: 100–5,000 mg/L, OP dose: 5–25 g/L, and temperature: 298 K).

These clearly show that OP, a low-cost and bio-based adsorbent, can be used for removing anionic dyes (such as MO and CR) from aqueous solutions over a wide concentration range.

Table 3
Significance of various parameters on the adsorption of MO and CR by OP

Dye	Parameter	*p*-value	*f*-value
MO	pH	0.08488	4.59683
	Initial concentration	0.01810	41.32328
	OP dose	6.9×10^{-7}	25.82621
	Temperature	0.01448	7.63899
CR	pH	0.53505	0.43276
	Initial concentration	0.00042	16.00383
	OP dose	0.00250	11.11613
	Temperature	0.15067	2.29386

*p-value < 0.05 and f-value > 5: significant. p-value > 0.05 and f-value < 5: insignificant.

3.5. Adsorption kinetics

Adsorption kinetics is important to identify the steps and parameters controlling the rate of the adsorption process. Three different models (pseudo-first-order (PFO), pseudo-second-order (PSO), and Elovich kinetic models [54–56]) were employed to elucidate the mechanism of MO or CR adsorption onto OP in this study. The linearized equation of the PFO kinetic model is represented in Eq. (5):

$$\log(q_e - q_t) = \log q_e - \frac{k_1}{2.303} \cdot t \tag{5}$$

where q_e and q_t (mg/g) refer to the capacities at equilibrium and contact time t (min), respectively; and k_1 (1/min) is the PFO rate constant. These were derived from the slopes and intercepts obtained by the "$\log(q_e - q_t)$ vs. t" graphs and are exhibited in Table 5 with the determination coefficients (R^2). The R^2 values with this model were equal to 0.9425 and 0.8553 for the adsorption of MO and CR, respectively. These are lower than those obtained with the other kinetic models. Moreover, the calculated adsorption capacities were

Table 4
Maximum adsorption capacity (q_{max}) values for the removal of CR and MO using adsorbents reported in the literature

Dye	Adsorbent Type	q_{max} (mg/g)	Reference
MO	Olive pomace	257.4	Present study
MO	Waste banana peel	21.0	[42]
MO	Waste orange peel	20.5	[42]
MO	Almond shell residues	32.8	[43]
CR	Olive pomace	145.0	Present study
CR	Waste banana peel	18.2	[42]
CR	Waste orange peel	14.0	[42]
CR	Activated carbon prepared from coir pith	6.7	[44]
CR	Activated carbon (LR)	1.9	[45]
CR	Neem leaf powder	41.2	[46]
CR	Bagasse fly ash	11.9	[47]
CR	Tamarind fruit shell	10.5	[48]
CR	Acid activated red mud	7.1	[49]
CR	Cashew nut shell	5.2	[50]
CR	Activated carbon from *Myrtus communis* (AC–MC)	10.0	[51]
CR	Activated carbon from pomegranate (AC–PG)	19.2	[51]
CR	Raw pine cone	19.2	[52]
CR	Acid-treated pine cone	40.2	[52]
CR	Bengal gram seed husk	41.7	[53]

Table 5
Constants and R^2 values of the kinetic models for the adsorption of MO and CR using OP (initial dye concentration: 250 mg/L, OP dose: 10 g/L, and temperature: 298 K)

		Pseudo-first-order			Pseudo-second-order			Elovich		
Dye	$q_{e,exp}$ (mg/g)	k_1 (1/min)	$q_{e,cal}$ (mg/g)	R^2	k_2 (g/mg min)	$q_{e,cal}$ (mg/g)	R^2	α (mg/g min)	β (g/mg)	R^2
MO	17.83	0.0122	2.84	0.9425	0.0104	18.05	0.9997	33,488.093	1.1201	0.9632
CR	12.05	0.0157	8.45	0.8553	0.0027	13.23	0.9870	0.557	2.0193	0.9532

different from the experimentally-determined values, indicating that the data cannot be explained with PFO kinetic model.

The Elovich model is useful for especially describing the chemical adsorption mechanisms. Its linearized equation is expressed in Eq. (6):

$$q_t = \beta \cdot \ln(\alpha \cdot \beta) + \beta \cdot \ln(t) \quad (6)$$

where α (mg/g min) and β (g/mg) refer to the initial adsorption rate and the desorption constant relevant to the surface coverage and energy, respectively. The values of α and β were determined from the intercepts and slopes of the linear plots of "q_t vs. ln(t)". The determination coefficients with this kinetic model were 0.9632 and 0.9532 for the adsorption of MO and CR, respectively (Table 5). They were higher than the values with the PFO kinetic model but significantly lower than those obtained with the PSO kinetic model. Hence, this model was not appropriate for describing the kinetic data.

The linearized equation of PSO kinetic model is exhibited in Eq. (7):

$$\frac{t}{q_t} = \frac{1}{k_2 \cdot q_e^2} + \frac{1}{q_e} \cdot t \quad (7)$$

where k_2 (g/mg·min) indicates the rate constant of PSO adsorption. The q_e and k_2 values were calculated from the intercepts and slopes of the graphs of "t/q_t vs. t" (Fig. 10). Table 5 shows that the R^2 values with the PSO kinetic model were 0.9997 and 0.9870 for the adsorption of MO and CR, respectively, and were the highest R^2 values obtained in this study. Moreover, there was a good match between the experimental and theoretical q_e values, especially for MO (Table 5). These clearly exhibit that the adsorption of these two anionic dyes onto the OP could be described with PSO kinetic model. This indicates that chemical or physiochemical interactions occur between the anionic dyes and OP surface [40,55]. These results and trends are consistent with previous reports using OP as an adsorbent [16,18,20,21].

3.6. Intraparticle diffusion

Weber and Morris [57] proposed that kinetic models are inadequate for the expression of the diffusion mechanisms and steps that occur in the adsorption processes. The authors recommended an equation. Accordingly, the adsorption capacity varies with $t^{0.5}$ (Eq. 8):

$$q_t = k_{id} \cdot t^{0.5} + I \quad (8)$$

where k_{id} (mg/g min) and I (mg/g) refer to the rate constant of intraparticle diffusion (ID) and the thickness of the boundary layer, respectively. If the ID controls the process, the graph of "q_t vs. $t^{0.5}$" is linear and the k_{id} and I can be obtained by using the intercept and slope, respectively (Table 6). Table 6 and Fig. 11 show that ID was present in the adsorption of MO and CR onto OP since linear relationships were obtained for both separation systems. However, it was not the only mechanism since the lines did not pass through the origin [9,57].

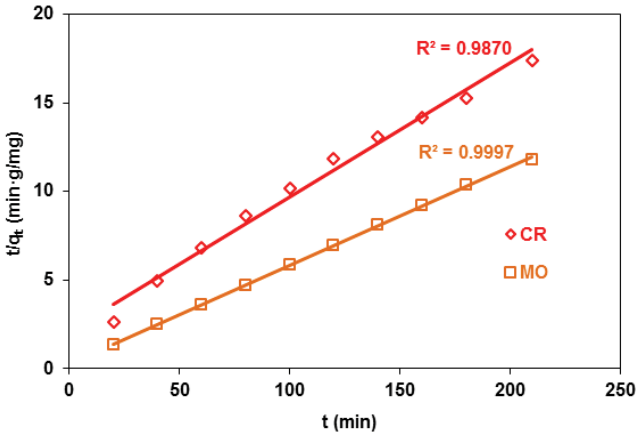

Fig. 10. Graphs of the PSO kinetic model for the adsorption of MO and CR by using OP (initial dye concentration: 250 mg/L, OP dose: 10 g/L, and temperature: 298 K).

Table 6
Parameters and R^2 values of the intraparticle diffusion model for the adsorption of MO and CR by OP (initial dye concentration: 250 mg/L, OP dose: 10 g/L, and temperature: 298 K)

Dye	k_{id} (mg/g min$^{0.5}$)	I (mg/g)	R^2
MO	0.248	14.351	0.8952
CR	0.477	5.140	0.9888

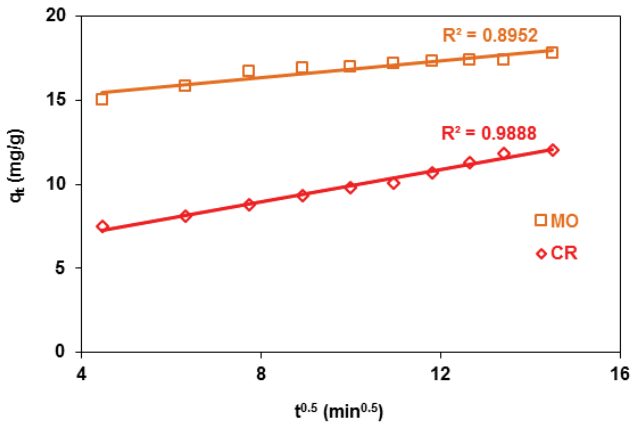

Fig. 11. Plots of the ID model for the adsorption of MO and CR onto OP (initial dye concentration: 250 mg/L, OP dose: 10 g/L, and temperature: 298 K).

3.7. Adsorption isotherms

The isotherm of a solid–liquid adsorption system generally provides information about the distribution of the adsorbate molecules on the adsorbent surface. This enables us to understand the type of interaction between the adsorbent surface and adsorbate [58]. The Langmuir, Freundlich, and Temkin isotherm models were tested in this study. The details of these isotherm models are well-documented in the literature [59–65].

The Langmuir isotherm model is the most common model used for the solid–liquid adsorption systems. It assumes a monolayer formation on the solid surface as well as the sorption of only one entity on each available site. Moreover, the binding energy on each site is equivalent and the interaction between the adsorbed molecules is negligible [61–63]. The equation of the Langmuir model is shown in Eq. (9):

$$q_e = \frac{Q_{\max} \cdot K_L \cdot C_e}{1 + K_L \cdot C_e} \tag{9}$$

where $Q_{\max}$ (mg/g) and K_L (L/mg) refer to the theoretical value of maximum adsorption capacity and the Langmuir adsorption constant, respectively. The R^2 values for this isotherm model were 0.9533 and 0.7921 for the sorption of MO and CR, respectively (Table 7). However, these were not the maximum values obtained in this study. This indicated that the model could not explain the behavior of MO and CR adsorption on the OP surface.

The Freundlich isotherm is an empirical equation applicable to the physical adsorption processes that generally occur on heterogeneous surfaces and can express heterogeneity of the surface and the multi-layer distribution of the molecules on the OP [64]. The Freundlich equation is given in Eq. (10):

$$q_e = K_f \cdot C_e^{1/n} \tag{10}$$

where K_f (L/mg) and n are Freundlich isotherm model constants. The value of "$1/n$" indicates the behavior of the process as irreversible ($1/n = 0$), favorable ($0 < 1/n < 1$), or unfavorable ($1/n > 1$). In this study, the highest R^2 values were obtained with this model in the isotherm analysis (Table 7). These were 0.9802 and 0.9469 for the adsorption of MO and CR, respectively (Fig. 12). In particular, the R^2 value obtained with CR was much higher than those with the other models tested. Therefore, this isotherm model was considered to be acceptable to describe the adsorption of MO and CR onto OP. In other words, a multilayer adsorption process could occur on the heterogeneous surface of the OP. The process was predicted to be favorable since $1/n$ was between zero and one for both dyes studied. These trends are consistent with the results of the studies using OP for the adsorption of synthetic dyes [17,19,21,30].

According to the Temkin isotherm model, indirect contact between the solute molecules in the adsorption process is important. The model assumes that the adsorption heat decreases with the surface covering [65]. The equation of Temkin isotherm is shown in Eq. (11):

$$q_e = B_1 \ln K_T + B_1 \ln C_e \tag{11}$$

where B_1 (J/mol) and K_T (L/mg) are the Temkin coefficient related to the heat of adsorption and the equilibrium binding constant, respectively. The values of K_T and B_1 can be calculated from the plot of "q_e vs. lnC_e". The R^2 values with this model were 0.9063 and 0.7391 for the adsorption of MO and CR, respectively, and were lower than those obtained with the other two isotherm models.

3.8. Effect of temperature and thermodynamics

The influence of temperature on the adsorption of MO and CR by using OP is exhibited in Fig. 13. This shows that increasing the temperature of the system decreased the adsorption efficiency. This is consistent with the literature and is likely owing to the exothermic nature of the system and physical interactions between the adsorbate and adsorbent [8,66]. The effect was significant for MO adsorption ($p < 0.05$ and $f > 5$, Table 3), but not significant for CR uptake ($p >> 0.05$ and $f < 5$, Table 3).

The changes in the Gibbs free energy ($\Delta G°$), enthalpy ($\Delta H°$), and entropy ($\Delta S°$) were calculated employing the relevant data and Eqs. (12) and (13):

$$\Delta G° = -RT \ln K_L \tag{12}$$

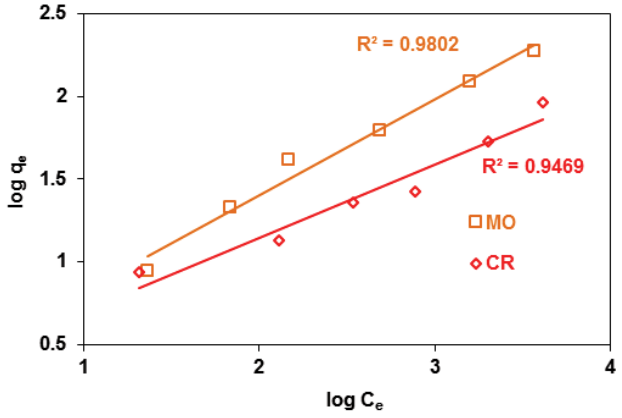

Fig. 12. Graphs of Freundlich isotherm model for the adsorption of MO and CR by OP at 298 K (initial dye concentration: 100–5,000 mg/L, OP dose: 10 g/L, and temperature: 298 K).

Table 7
Constants and R^2 values of the Langmuir, Freundlich, and Temkin isotherm models for the adsorption of MO and CR onto OP (initial dye concentration: 100–5,000 mg/L, OP dose: 10 g/L, and temperature: 298 K)

Dye	Langmuir			Freundlich			Temkin		
	$Q_{\max}$ (mg/g)	K_L (L/mg)	R^2	$1/n$	K_f (L/mg)	R^2	B_1 (J/mol)	K_T (L/mg)	R^2
MO	217.390	0.00125	0.9533	0.4401	1.758	0.9802	33.860	0.0300	0.9063
CR	107.527	0.00080	0.7921	0.5780	1.849	0.9469	14.160	0.0303	0.7391

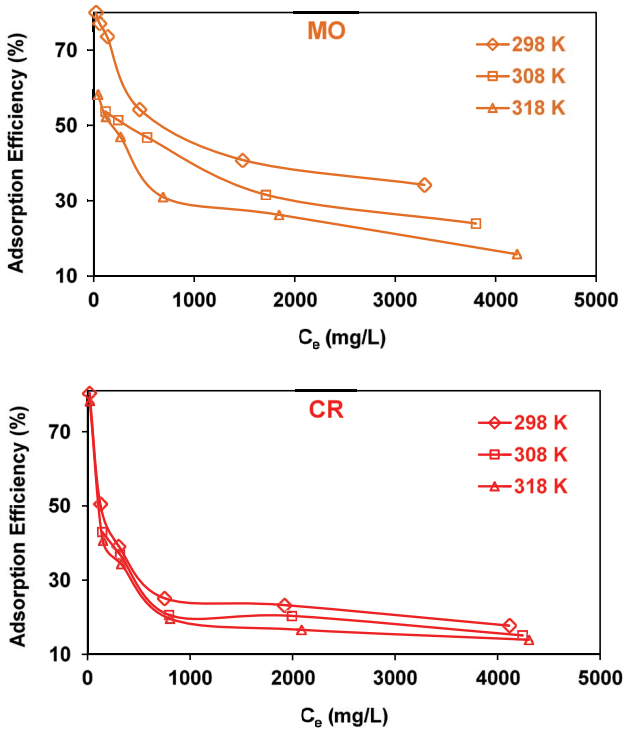

Fig. 13. Influence of temperature on the adsorption of MO and CR by OP (initial dye concentration: 100–5,000 mg/L, OP dose: 10 g/L, and temperature: 298–318 K).

Table 8
Thermodynamic parameters for the adsorption of MO and CR by using OP (initial dye concentration: 100–5,000 mg/L, OP dose: 10 g/L, and temperature: 298–318 K)

Dye	T (K)	ΔG°_{ads} (kJ/mol)	ΔH°_{ads} (kJ/mol)	ΔS°_{ads} (kJ/mol K)
MO	298	16.562	–9.334	–0.087
	308	18.260		
	318	17.020		
CR	298	17.517	–1.965	–0.660
	308	18.425		
	318	18.989		

$$\ln K_L = -\frac{\Delta H^\circ}{RT} + \frac{\Delta S^\circ}{R} \quad (13)$$

where K_L (L/mg) is the Langmuir constant at temperature T. In general, the ΔG° for physical adsorption processes varies between 0 and 20 kJ/mol. The range is about 80–400 kJ/mol for chemical processes [63,67,68]. The values of the thermodynamic parameters are shown in Table 8. It indicates that the adsorption of MO or CR onto OP might be due to the physical or physico-chemical interactions. The process was assumed to be non-spontaneous for both dyes due to the positive ΔG° values. The ΔH° and ΔS° values were obtained from the slopes and intercepts, respectively, of the graphs of "$\ln K_L$ vs. $1/T$". The negative ΔH° values confirmed the exothermic nature and feasibility of the separation, and are consistent with the previous studies in the literature [69,70]. Furthermore, the negative ΔS° values exhibited that the randomness at the interface decreased during the adsorption process.

4. Conclusion

The aim of this study was to test the use of olive pomace (OP) for the adsorption of two anionic dyes, Methyl Orange (MO) and Congo Red (CR), from aqueous solutions. It was observed that the effect of the pH on the process was not significant indicating that OP can be efficiently used over a wide pH range. Hence, the effects of other system parameters were investigated without pH adjustment of the dye solutions. Equilibration times for the adsorption of the dyes onto OP were identical at about 210 min. The maximum adsorption capacity for MO (q_{max} = 257.4 mg/g) was higher than that for CR (q_{max} = 145.0 mg/g). Both values were higher than those previously obtained from earlier investigations using various waste materials and by-products for the adsorption of these dyes. The adsorption capacity decreased with the OP dosage and increased with the initial MO or CR concentration. The PSO and ID models were well correlated with the experimental data. The maximum R^2 values were obtained with the Freundlich isotherm model and were R^2 = 0.9802 and 0.9469 for the adsorption of MO and CR, respectively. Therefore, the mechanism was considered to be consistent with this isotherm model. Increasing the temperature negatively influenced the adsorption efficiency. Thermodynamic parameters showed the possible formation of physical or physico-chemical interactions between the anionic dyes and OP. The negative ΔH° values indicated the exothermic nature of the system. The overall results showed that OP is an effective and low-cost bio-based adsorbent that can be used during the separation of anionic dyes such as MO and CR from aqueous solutions over wide pH and concentration ranges.

Funding

The authors are thankful to Selçuk University for funding under Grant Number 16201045. The authors also would like to thank Prof. Dr. Celalettin Ozdemir for the gift of the olive pomace.

Symbols and abbreviations

AE	—	Adsorption efficiency
B	—	Temkin equilibrium binding constant, J/mol
BET	—	Brunauer–Emmett–Teller method
BJH	—	Barrett–Joyner–Halenda method
C_0	—	Initial concentration of dye, mg/L
C_e	—	Equilibrium concentration of dye, mg/L
C_t	—	Concentration of dye at time t, mg/L
CR	—	Congo red
EDX	—	Energy-dispersive X-ray
FTIR	—	Fourier transformed infrared spectroscopy

I	—	Boundary layer diffusion effects, mg/g
ID	—	Intraparticle diffusion
k_1	—	PFO rate constant, 1/min
k_2	—	PSO rate constant, g/mg min
k_{id}	—	ID rate constant, mg/g $min^{0.5}$
K_F	—	Freundlich adsorption capacity, L/mg
K_L	—	Langmuir equilibrium constant, L/mg
K_T	—	Temkin constant related to the adsorption heat, L/mg
m	—	Mass of OP, g
MO	—	Methyl orange
n	—	Freundlich adsorption intensity
OP	—	Olive pomace
PFO	—	Pseudo-first-order
pH_{ZPC}	—	pH at the zero-point charge
PSO	—	Pseudo-second-order
q_e	—	Amount of dye adsorbed per gram adsorbent at equilibrium, mg/g
q_t	—	Amount of dye adsorbed per gram adsorbent at time t, mg/g
q_{max}	—	Maximum amount of dye adsorbed per gram adsorbent, mg/g
R	—	Gas constant, 8.314 J/mol K
R^2	—	Determination coefficient
SEM	—	Scanning electron microscopy
t	—	Time, minute
T	—	Temperature, K or °C
V	—	Volume of the aqueous solution, L
α	—	Elovich initial adsorption rate, mg/g min
β	—	Elovich desorption constant, g/mg
$\Delta G°$	—	Change in Gibbs free energy, kJ/mol
$\Delta H°$	—	Change in enthalpy, kJ/mol
$\Delta S°$	—	Change in entropy, kJ/mol K

References

[1] M. Goto, N. Hayashi, S. Goto, Adsorption and desorption of phenol on anion-exchange resin and activated carbon, Environ. Sci. Technol., 20 (1986) 463–467.

[2] J.P. Jadhav, S.S. Phugare, R.S. Dhanve, S.B. Jadhav, Rapid biodegradation and decolorization of Direct Orange 39 (Orange TGLL) by an isolated bacterium *Pseudomonas aeruginosa* strain BCH, Biodegradation, 21 (2010) 453–463.

[3] R. Azargohar, A.K. Dalai, Production of activated carbon from luscar char: experimental and modeling studies, Microporous Mesoporous Mater., 85 (2005) 219–225.

[4] O.S. Bello, K.A. Adegoke, A.A. Olaniyan, H. Abdulazeez, Dye adsorption using biomass wastes and natural adsorbents: overview and future prospects, Desal. Water Treat., 53 (2013) 1–24.

[5] G. Crini, Non-conventional low-cost adsorbents for dye removal: a review, Bioresour. Technol., 97 (2006) 1061–1085.

[6] R. Karthik, R. Muthezhilan, A.H. Jaffar, K. Ramalingam, V. Rekha, Effective removal of Methylene Blue dye from water using three different low-cost adsorbents, Desal. Water Treat., 57 (2015) 10626–10631.

[7] M.A. Abdel-Khalek, M.K. Abdel Rahman, A.A. Francis, Exploring the adsorption behavior of cationic and anionic dyes on industrial waste shells of egg, J. Environ. Chem. Eng., 5 (2017) 319–327.

[8] Y.S. Ho, T.H. Chiang, Y.M. Hsueh, Removal of basic dye from aqueous solution using tree fern as a biosorbent, Process Biochem., 40 (2005) 119–124.

[9] J. Liu, F. Chen, C. Li, L. Lu, C. Hu, Y. Wei, P. Raymer, Q. Huang, Characterization and utilization of industrial microbial waste as novel adsorbent to remove single and mixed dyes from water, J. Cleaner Prod., 208 (2018) 552–562.

[10] W. Shi, H. Ren, X. Huang, M. Li, Y. Tang, F. Guo, Low cost red mud modified graphitic carbon nitride for the removal of organic pollutants in wastewater by the synergistic effect of adsorption and photocatalysis, Sep. Purif. Technol., 237 (2020) 116477–116484.

[11] F. Pagnanelli, S. Mainelli, F. Veglio, L. Toro, Heavy metal removal by olive pomace: biosorbent characterization and equilibrium modeling, Chem. Eng. Sci., 58 (2003) 4709–4717.

[12] S.H. Gharaibeh, W.Y. Abu-el-sha'r, M.M. Al-Kofahi, Removal of selected heavy metals from aqueous solutions using processed solid residue of olive mill products, Water Res., 32 (1998) 498–502.

[13] Y. Nuhoğlu, E. Malkoç, Thermodynamic and kinetic studies for environmentally friendly Ni(II) biosorption using waste pomace of olive oil factory, Bioresour. Technol., 100 (2009) 2375–2380.

[14] V. Rizzi, F. D'Agostino, P. Fini, P. Semeraro, P. Cosma, An interesting environmental friendly clean-up: the excellent potential of olive pomace for disperse blue adsorption/desorption from wastewater, Dyes Pigm., 140 (2017) 480–490.

[15] F. Pagnanelli, S. Mainelli, S. De Angelis, L. Toro, Biosorption of protons and heavy metals onto olive pomace: modelling of competition effects, Water Res., 39 (2005) 1639–1651.

[16] T. Akar, I. Tosun, Z. Kaynak, E. Ozkara, O. Yeni, E.N. Sahin, S.T. Akar, An attractive agro-industrial by-product in environmental clean-up: dye biosorption potential of untreated olive pomace, J. Hazard. Mater., 166 (2009) 1217–1225.

[17] H. Bozkan, The Removal of Azo Dyes by Using Olive Waste (Pomace) and Adsorption Method, MS Thesis, Selçuk University, Konya, Turkey, 2012.

[18] S. Dağdelen, B. Acemioğlu, E. Baran, O. Koçer, Removal of Remazol Brilliant Blue R from aqueous solution by pirina pretreated with nitric acid and commercial activated carbon, Water Air Soil Pollut., 225 (2014) 1899–1913.

[19] O. Koçer, B. Acemioğlu, Adsorption of Basic Green 4 from aqueous solution by olive pomace and commercial activated carbon: process design, isotherm, kinetic and thermodynamic studies, Desal. Water Treat., 57 (2015) 16653–16669.

[20] M.K. Oden, S. Şahinkaya, S. Küçükçongar, Colour removal with adsorption process using pomace, Cumhuriyet Sci. J., 38 (2017) 215–219.

[21] W.S. Beaj, A.A. Omar, N.A. Ahmad, H.A. Alhinsheeri, S.M. Abdulnabi, M.F. Sheemah, Adsorption of Methyl Orange from Aqueous Solutions using Olive Pomace: A Kinetic and Isotherm Study, The 3rd Annual Conference on Theories and Applications of Basic and Biosciences, Misurata, Libya, 2019, pp. 23–33.

[22] S. Brunaur, P.H. Emmett, E. Teller, Adsorption of gases in multimolecular layers, J. Am. Chem. Soc., 60 (1938) 309–319.

[23] E.P. Barrett, L.G. Joyner, P.P. Halenda, The determination of pore volume and area distributions in porous substances. I. Computations from nitrogen isotherms, J. Am. Chem. Soc., 73 (1951) 373–380.

[24] L.S. Balistrieri, J.W. Murray, The surface chemistry of goethite (–FeOOH) in major ion seawater, Am. J. Sci., 281 (1981) 788–806.

[25] H. Chen, J. Zhao, G. Dai, Silkworm exuviae—a new non-conventional and low-cost adsorbent for removal of methylene blue from aqueous solutions, J. Hazard. Mater., 186 (2011) 1320–1327.

[26] Y. Zhang, M. Yang, X.M. Dou, H. He, D.S. Wang, Arsenate adsorption on an Fe–Cebimetal oxide adsorbent: role of surface properties, Environ. Sci. Technol., 39 (2005) 7246–7253.

[27] D.P. Dutta, R. Venugopalan, S. Chopade, Manipulating carbon nanotubes for efficient removal of both cationic and anionic dyes from wastewater, ChemistrySelect, 2 (2017) 3878–3888.

[28] X. Han, W. Wang, X. Ma, Adsorption characteristics of Methylene Blue onto low cost biomass material lotus leaf, Chem. Eng. J., 171 (2011) 1–8.

[29] H. Bensalah, S.A. Younssi, M. Ouammou, A. Gurlo, M.F. Bekheet, Azo dye adsorption on an industrial waste-transformed hydroxyapatite adsorbent: kinetics, isotherms, mechanism and regeneration studies, J. Environ. Chem. Eng., 8 (2020) 103807–103816.

[30] N.M. Mohammad, A. Taghizadeh, M. Taghizadeh, M.A.S. Baglou, Surface modified montmorillonite with cationic surfactants: preparation, characterization, and dye adsorption from aqueous solution, J. Environ. Chem. Eng., 7 (2019) 1–11.,
[31] M.M. Souza, T.N.S. Pereira, A.P. Viana, M.G. Pereira Junior, A.T. do Amaral Júnior, H.C. Madureira, Flower receptivity and fruit characteristics associated to time of pollination in the yellow passion fruit *Passiflora edulis* Sims f. *flavicarpa* Degener (Passifloraceae), Sci. Hortic., 101 (2008) 313–385.
[32] F. Pagnanelli, C.C. Viggi, M. Sara, L. Toro, Valorisation of Olive Oil Solid Wastes for the Development of New Biosorbents for Heavy Metals, 4th European Bioremediation Conference, Chania, Crete, Greece, 2008.
[33] M. Mohammadi, A.J. Hassani, A.R. Mohamed, G.D. Najafpour, Removal of Rhodamine B from aqueous solution using Palm Shell-based Activated Carbon: adsorption and kinetic studies, J. Chem. Eng. Data, 55 (2010) 5777–5785.
[34] V. Ponnusami, S. Vikram, S.N. Srivastava, Guava (*Psidium guajava*) leaf powder: novel adsorbent for removal of methylene blue from aqueous solutions, J. Hazard. Mater., 152 (2008) 276–286.
[35] A. Roy, S. Chakraborty, S.P. Kundu, B. Adhikari, S.B. Majumder, Adsorption of anionic-azo dye from aqueous solution by lignocellulose-biomass jute fiber: equilibrium, kinetics, and thermodynamics study, Ind. Eng. Chem. Res., 51 (2012) 12095−12106.
[36] K.Diouri, A. Kherbeche, A. Chaqroune, Kinetics of Congo Red dye adsorption onto marble powder sorbents, Int. J. Innovative Res. Sci. Eng. Technol., 4 (2015) 267–274.
[37] D. Lin, B. Xing, Adsorption of phenolic compounds by carbon nanotubes: role of aromaticity and substitution of hydroxyl groups, Environ. Sci. Technol., 42 (2008) 7254–7259.
[38] A.K. Mishra, T. Arockiadoss, S. Ramaprabhu, Study of removal of azo dye by functionalized multi-walled carbon nanotubes, Chem. Eng. J., 162 (2010) 1026–1034.
[39] K. Boutemak, N. Taoualit, B. Cheknane, O. Laslouni, S. Djeddou, K. Medaoud, I. Mazouni, S. Aoudj, Equilibrium, kinetic and thermodynamic study of Green Malachite and Rhodamine-B dyes sorption on olive pomace, Chem. Eng. Trans., 73 (2019) 277–282.
[40] H. Zeidan, M.E. Marti, Separation of formic acid from aqueous solutions onto anion exchange resins: Equilibrium, kinetic, and thermodynamic data, J. Chem. Eng. Data, 64 (2019) 2718−2727.
[41] S. Chen, J. Zhang, C. Zhang, Q. Yue, Y. Li, C. Li, Equilibrium and kinetic studies of Methyl Orange and Methyl Violet adsorption on activated carbon derived from phragmites australis, Desalination, 252 (2010) 149–156.
[42] G. Annadurai, R.L. Juang, D.J. Lee, Use of cellulose-based wastes for adsorption of dyes from aqueous solutions, J. Hazard. Mater., 92 (2002) 263–274.
[43] F. Deniz, Dye removal by almond shell residues: studies on biosorption performance and process design, Mater. Sci. Eng., C, 33 (2013) 2821–2826.
[44] C. Namasivayam, D. Kavitha, Removal of Congo red from water by adsorption onto activated carbon prepared from coir pith, an agricultural solid waste, Dyes Pigm., 54 (2002) 47–58.
[45] A. Aygun, S.Yenisoy-Karakas, I. Duman, Production of granular activated carbon from fruit stones and nutshells and evaluation of their physical, chemical and adsorption properties, Microporous Mesoporous Mater., 66 (2003) 189–195.
[46] K.G. Bhattacharyya, A. Sharma, Azadirachta indica leaf powder as an effective biosorbent for dyes: a case study with aqueous Congo Red solutions, J. Environ. Manage., 71 (2004) 217–229.
[47] I.D. Mall, V.C. Srivastava, N.K. Agarwal, I.M. Mishra, Removal of Congo Red from aqueous solution by bagasse fly ash and activated carbon: kinetic study and equilibrium isotherm analyses, Chemosphere, 61 (2005) 492–501.
[48] M.C. Reddy, Removal of direct dye from aqueous solution with an adsorbent made from tamarind fruit shell, an agricultural solid waste, J. Sci. Ind. Res., 65 (2006) 443–446.
[49] A. Tor, Y. Cengeloglu, Removal of Congo Red from aqueous solution by adsorption onto acid activated red med, J. Hazard. Mater., 138 (2006) 409–415.
[50] P.S. Kumar, S. Ramalingam, C. Senthamarai, M. Niranjanna, P. Vijayalakshmi, S. Sivanesan, Adsorption of dye from aqueous solution by cashew nut shell: Studies on equilibrium isotherm, kinetics and thermodynamics of interactions, Desalination, 261 (2010) 52–60.
[51] M. Ghaedi, H. Tavallali, M. Sharifi, S.N. Kokhdan, A. Asghari, Preparation of low cost activated carbon from *Myrtus communis* and pomegranate and their efficient application for removal of Congo Red from aqueous solution, Spectrochim. Acta, Part A, 86 (2012) 107–114.
[52] S. Dawood, T.K. Sen, Removal of anionic dye Congo Red from aqueous solution by raw pine and acid-treated pine cone powder as adsorbent: equilibrium, thermodynamic, kinetics, mechanism and process design, Water Res., 46 (2012) 1933–1946.
[53] M.C.S. Reddy, V. Nirmala, C. Ashwini, Bengal Gram Seed Husk as an adsorbent for the removal 524 of dye from aqueous solutions–Batch studies, Arabian J. Chem., 10 (2017) 2554–2566.
[54] S.Y. Lagergren, Zur theorie Der Sogenannten adsorption geloster stoffe, Kungl. Svens. Vetenskapsakad., 24 (1898) 1–39.
[55] Y.S. Ho, G. Mckay, Pseudo-second-order model for sorption processes, Process Biochem., 34 (1999) 451–465.
[56] S.Y. Elovich, O.G. Larinov, Theory of adsorption from solutions of non-electrolytes on solid (I) equation adsorption from solutions and the analysis of its simplest form, (II) verification of the equation of adsorption isotherm from solutions, Izvestiya Akademii Nauk. SSSR, Otdelenie Khimicheskikh Nauk, 2 (1962) 209–216.
[57] W.J. Weber, J.C. Morris, Water Pollution Symposium, Proceedings of 1st International Conference on Water Pollution Research, Vol. 2, Pergamon, Oxford, 1962, pp. 231–266.
[58] D. Kavitha, C. Namasivayam, Experimental and kinetic studies on Methylene Blue adsorption by coir pith carbon, Bioresour. Technol., 98 (2007) 14–21.
[59] A. Khaled, A.E. Nemr, A. El-Sikaily, O. Abdelwahab, Treatment of artificial textile dye effluent containing Direct Yellow 12 by orange peel carbon, Desalination, 238 (2009) 210–232.
[60] P. Murugan, S.T. Ramesh, V.M. Biju, Characterization, morphology and stability assessment of low-cost industrial by-product as an adsorbent for the removal of methylene blue from aqueous solution, Sep. Sci. Technol., 55 (2020) 471–486.
[61] I. Langmuir, The constitution and fundamental properties of solids and liquids, Part I. Solids, J. Am. Chem. Soc., 38 (1916) 2221–2295.
[62] K.K.H. Choy, J.F. Porter, G. McKay, Langmuir isotherm models applied to the multicomponent sorption of acid dyes from effluent onto activated carbon, J. Chem. Eng. Data, 45 (2000) 575–584.
[63] H. Zeidan, D. Ozdemir, N. Kose, E. Pehlivan, G. Ahmetli, M.E. Marti, Separation of formic acid and acetic acid from aqueous solutions using sugar beet processing fly ash: characterization, kinetics, isotherms and thermodynamics, Desal. Water Treat., 202 (2020) 283–294.
[64] H.M.F. Freundlich, Adsorption in solution, Z. Phys. Chem., 57 (1906) 385–490.
[65] M. Temkin, V. Pyzhev, Kinetics of ammonia synthesis on promoted iron catalysts, Acta Phys., 12 (1940) 217–222.
[66] K.K. Panday, G. Prasad, V.N. Singh, Use of wollastonite for the treatment of Cu(II) rich effluents, Water Air Soil Pollut., 27 (1986) 287–296.
[67] M.J. Jaycock, G.D. Parfitt, Chemistry of Interfaces, Ellis Horwood Ltd., Chichester, 1981.
[68] C.E. Can, Separation of Itaconic Acid from Aqueous Phases Using Anionic Resins, MS Thesis, Selçuk University, Konya, Turkey, 2018.
[69] H. Kaur, A. Thakur, Adsorption of Congo Red dye from aqueous solution onto ash of Cassia Fistula seeds: kinetic and thermodynamic studies, Chem. Sci. Rev. Lett., 3 (2014) 159–169.
[70] F. Krika, O.F. Benlahbib, Removal of Methyl Orange from aqueous solution via adsorption on cork as a natural and low-cost adsorbent: equilibrium, kinetic and thermodynamic study of removal process, Desal. Water Treat., 53 (2014) 3711–3723.